Spectroscopic orbits and spectral variations of RS OPHIUCHI

E. Brandi[1,2,3], C. Quiroga[1,2], O.E. Ferrer[1,4], J. Mikołajewska[5], L.G. García[1,2]

[1]Facultad de Ciencias Astronómicas y Geofísicas, Universidad Nacional de La Plata (UNLP), Argentine
[2] Instituto de Astrofísica de La Plata (UNLP-CONICET), Argentine
[3]Comisión de Investigaciones Científicas de la Provincia de Buenos Aires (CIC), Argentine
[4]Consejo Nacional de Investigaciones Científicas y Técnicas (CONICET), Argentine
[5]Copernicus Astronomical Center, Warsaw, Poland

contact e-mail: ebrandi@fcaglp.unlp.edu.ar

1.- Introduction

We performed an analysis of around thirty optical and near infrared spectra of RS Oph obtained at CASLEO, San Juan, Argentina, with the echelle REOSC spectrograh attached to the 2.15m telescope, since 1998 to October 2006. The spectroscopic orbits have been obtained measuring the radial velocities from the absorption lines of the cool component and from the broad emission wings of the H I which seem to be associated with the hot component. A set of blue absorption lines were also analized in order to connect them with the hot component motion.
Spectral variations related to the 2006 outburst are presented. In particular optical and near infrared spectroscopy

obtained 53-55 and 242 days following the eruption.

2.- Spectroscopic orbits

On the basis of high resolution spectra (R∼12000) collected with the 2.15 m telescope of CASLEO at San Juan, Argentina, during the period 1998−2006, we have measured the radial velocities of the cool component from the M-type absorption lines, specially Fe I, Ti I, Ni I, Si I and Co I in the red region, λ ∼6000-8000 Å.

The Table 1 lists the resulting orbital solutions. For the M-giant we have obtained several solutions using only our radial velocities as well as our radial velocities combined with the Dobrzycka & Kenyon (1994, hereafter DK94) and Fekel et al. (2000, hereafter F00) data and considering weighted values of radial velocities in this case. The elliptical orbit fits the measured velocities slightly better than a circular one and we note that such eccentric solution is mainly induced by the CASLEO observations.

We have also measured the cF-type absorption lines in the blue region of our spectra (λ ∼4000-5800 Å),which are believed to be linked to the hot companion (e.g. Mikołajewska & Kenyon 1992; Quiroga et al. 2002; Brandi et al.2005). Only the stronger Ti II absorption lines were considered and not the Fe II ones because they show very variable and complex profiles along our observations. The individual radial velocities were obtained by gaussian fitting of the line profiles and a mean value was calculated for each spectrum.

The cF absorption lines trace not clearly the orbit of the hot component. Any orbital solution leads to significant

eccentricity (see Table 1) and the radial velocity curve is shifted by ∼-0.26 (0.74) relative to the M giant solution instead of 0.5P (Fig. 1). We think in agreement with DK94 that in RS Oph the cF absorptions are not associated with either binary component.

In addition, we have determined the radial velocities of the broad emission wings of Hα which would reflect the motion of the hot component if they were formed in the inner region of the accretion disk or in an extended envelope near the hot component (e.g. Quiroga et al. 2002). For this we have used the method outlined by Schneider & Young (1980).

The broad emission line wings of Hα, show a mean velocity similar to the red giant systemic velocity. They are clearly in antiphase with the M-giant curve which suggest that they are fomed in a region very near to the hot component . Two solutions are shown in Fig. 2, one is considering all the measured radial velocities and other the binned data, taking phase intervals of 0.05.

Finally we have calculated the combined orbital solutions with the M giant and the Hα emission wings (see Table 1). These solutions shows a clear antiphase variations of both sets of radial velocities and the systemic velocity agrees with that of the cool component orbital solutions. Taking the period as a free parameter for a circular orbit, a period of 454.1±0.41 days was obtained, very similar to that obtained for the M giant and the best combined solution leads to a lower eccentricity (e=0.04±0.03).

Combined solutions using the binned data are also pre-

sented in Table 1 and analogous results were obtained.

All the combined solutions presented in Table 1 for unbinned data, lead to a mass ratio $q = M_{\rm g}/M_{\rm h} = 0.59 \pm 0.05$, the component masses $M_{\rm g} \sin^3 i = 0.35\,{\rm M}_\odot$ and $M_{\rm h} \sin^3 i = 0.59\,{\rm M}_\odot$, and the binary separation $a \sin i = 240\,{\rm R}_\odot$.

Asuming that the hot component is a massive white dwarf close to the Chandrasekhar limit ($M_{\rm h} = 1.2 - 1.4{\rm M}_\odot$) the red giant mass results $M_{\rm g} = 0.68{-}0.80{\rm M}_\odot$ and the orbit inclination, $i = 49^\circ - 52^\circ$, which is consistent with the absence of eclipses in the optical light curve. We have also observed in our spectra the lack of eclipses in the HI and HeI emission line fluxes along the orbital phases.

We adopt the period of 453.6 days and the phases in the figures were calculated taken as zero phase, $T_\circ$, the time of the maximum positive velocity:

$$\mathrm{Max} = \mathrm{JD}\,2445156.94\,(\pm 5) + 453.6\,(\pm 0.4)\,\times \mathrm{E}. \qquad (1)$$

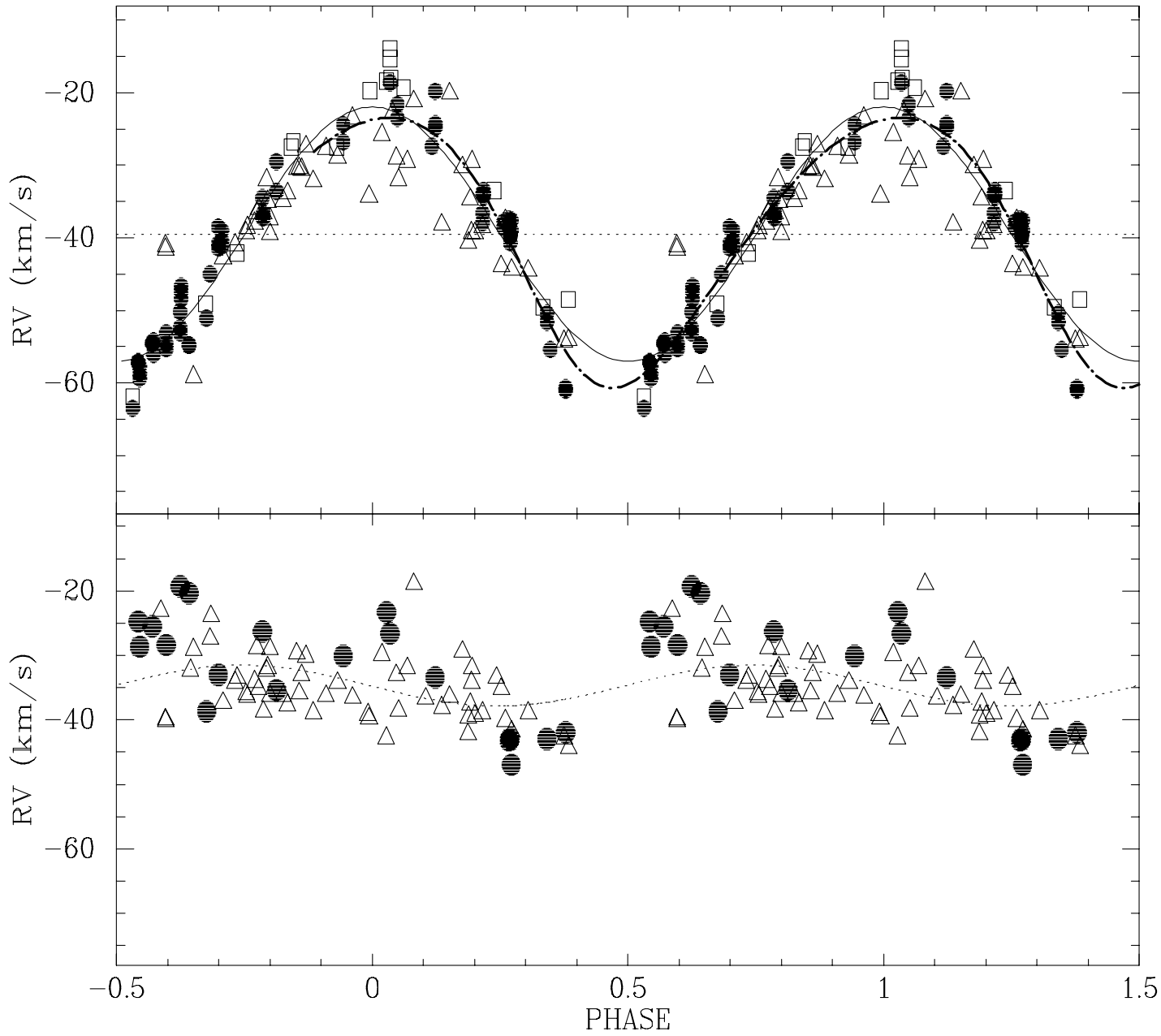

Figure 1: Phased radial velocity data and orbital solutions for RS Oph. Filled circles represent our data and open triangles and squares, the DK's and Fekel's data, respectively. The upper panel shows the velocity curve of the M giant absorptions. Solid line gives the best circular fit and dash-dot line gives the eccentric orbit (e=0.14). The lower panel shows the velocity curve of the cF absorption lines and the theoretical curve (dot line) for circular solution. These two sets of solutions should be 0.5P out of phase, but not 0.74P

3.- RS Oph at quiescence

The spectra of RS Oph show variability in the fluxes of the emission lines and the continuum at quiescence. Fluctuations in the fluxes are observed during the period covered by our observations, from September 1998 until Septembre 2005. Several authors have previously reported this behaviour of RS Oph, outside the eruptive episodes (see Anupama & Mikołajewska, 1999 and refences therein).

The spectra present essentially emission lines of H I, He I and [O I] at 6300 Å . In the observed members of the Balmer series, the broad emission is cut by a central absorption with a red peak always stronger than the blue one (Hα profiles for several epochs are shown in Fig. 3). This central absorption remains strong over the whole orbital cycle and the radial velocity is practically constant, -50$\pm$4 and -47$\pm$3 kms^{-1} in Hα and Hβ respectively. The same was observed in AR Pav (Quiroga et al., 2002) and FN Sgr (Brandi et al.,2005) where it was proposed that this central absorption is originated in a significant amount of neutral material bounding the nebula in the orbital plane.

Broad emission components were detected in the emission lines of He I during April 2004 and September 2005 (see Fig. 3, right panel) at velocities of the order of -100 kms^{-1}. The intensity of the He I emission lines and the presence of these broad components change quickly in a time scale of one or two days.

Fig. 4 presents the Hα fluxes against the m_{4800} magnitudes calculated from our spectra. The figure shows that a clear correlation between both data exists, meaning that the emission line variability is correlated with the hot component activity (Anupama & Mikołajewska, 1999).
RS Oph was in a high state during May 1999, when the star was relatively bright and the emission line fluxes reached a maximum value. Flickering observations were carried out in May 1999 with the Torino Photopolarimeter and the 2.15-m telescope at Casleo. Fig. 5 shows the differential photometric observations with an integration time of one hour at the five filters UBVRI, simultaneously.

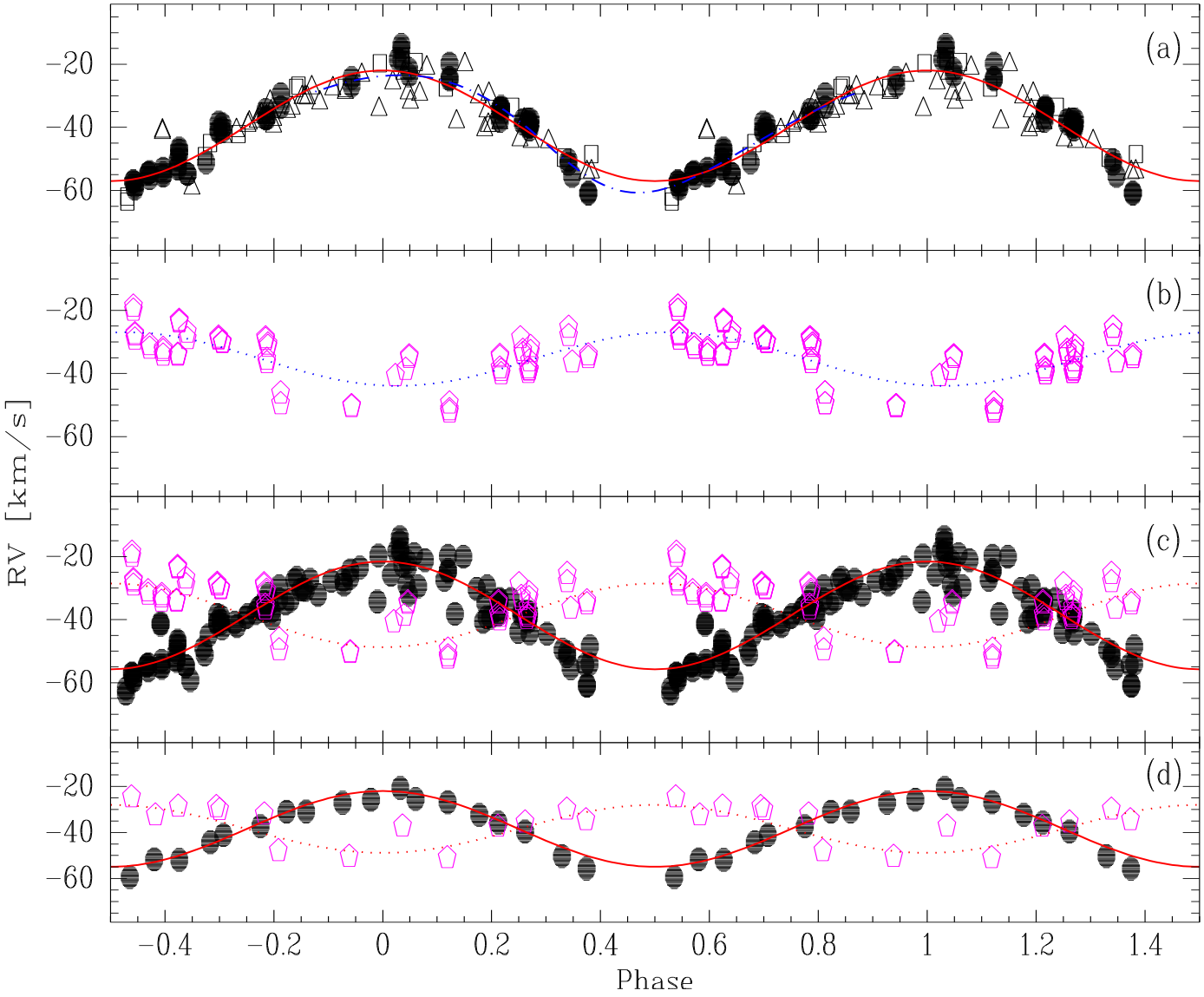

Figure 2: Phased radial velocity data and orbital solutions for RS Oph. Filled circles represent our data and open triangles and squares, the DK's and Fekel's data, respectively. (a) Velocity curve of the M-giant (same as Fig. 1). (b) Velocity curve of the Hα wings and the best circulat solution (red dot line). (c) Combined circular solution for the M-giant and the Hα wings. (d) The same with binned data.

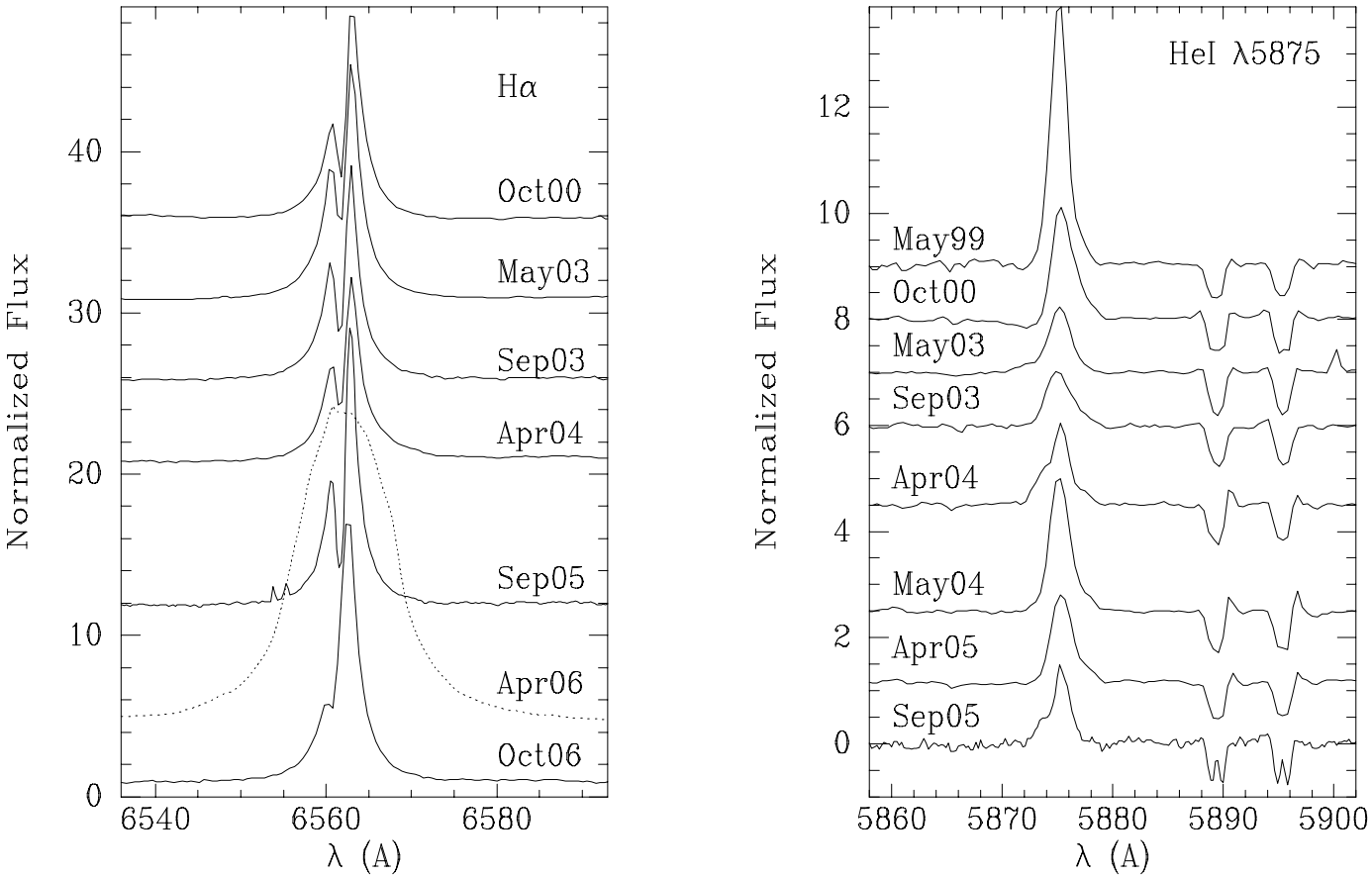

Figure 3: (*left panel*): Profiles of Hα. At quiescence the broad emission is cut by a permanent central absorption (RV=-50$\pm$4 kms^{-1}) which disappear during the outburst. This feature is appearing again in October 2006. (*right panel*): He Iλ5875 profiles during the quiescent period. Blueshifted broad components are observed on April 2004 and September 2005.

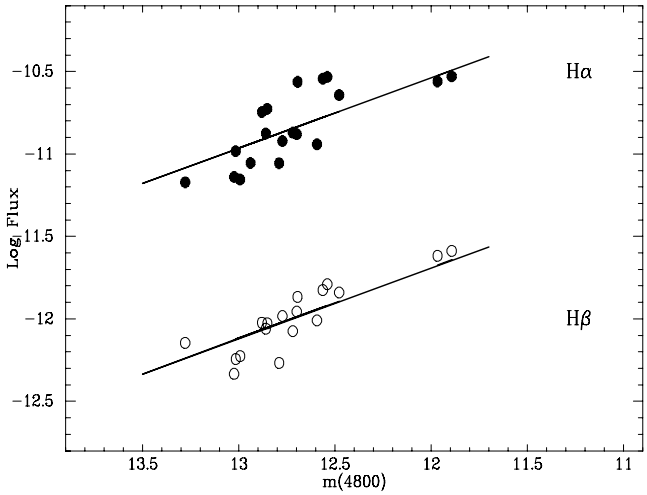

Figure 4: Correlation of the Hα and Hβ emission line fluxes with the magnitudes at 4800 Å measured from our spectra.

4.- RS Oph on April 2006

High-dispersion spectra of RS Oph were taken at Casleo with the same instrumental configuration on 2006 April 7-8 and October 12, that is, 53-55 and 240 days following the explosion, respectively.
The spectra of April show broad emission lines of hydrogen recombination lines, together with He I, He II, Fe II, N III, [O I]λ6300, [O III]λ5007, [N II]λ5754 and the Raman band at λ6825 Å .
The cF absorption system is not observed in April 2006.

Very narrow emission components are seen on the top of the broad emission components.
Strong coronal emission lines such as [Fe XIV]λ5305 and [Fe X]λ6375 (Fig. 6) are also present, showing the same structure in the profiles.

Our measures of the integrated fluxes, the radial velocity of the emission line components and the full width at zero intensity (FWZI) of several stronger lines are shown in Table 2.

The most of the emission lines present a strong and narrow component with a radial velocity between -14 and -25 kms^{-1} and two other components extended to the blue and the red side. In the cases of the [N II] and [O III] emission lines and the coronal lines, the radial velocity of the narrow component is more negative (-40 and -50 kms^{-1}).

We can see in Fig. 7 the He I and He II profiles showing a broad

pedestal with the strong narrow component at -15 and -23 kms^{-1} respectively. Two separate emission components of higher radial velocity are observed at ∼-200 and +150 kms^{-1} being the blue component stronger

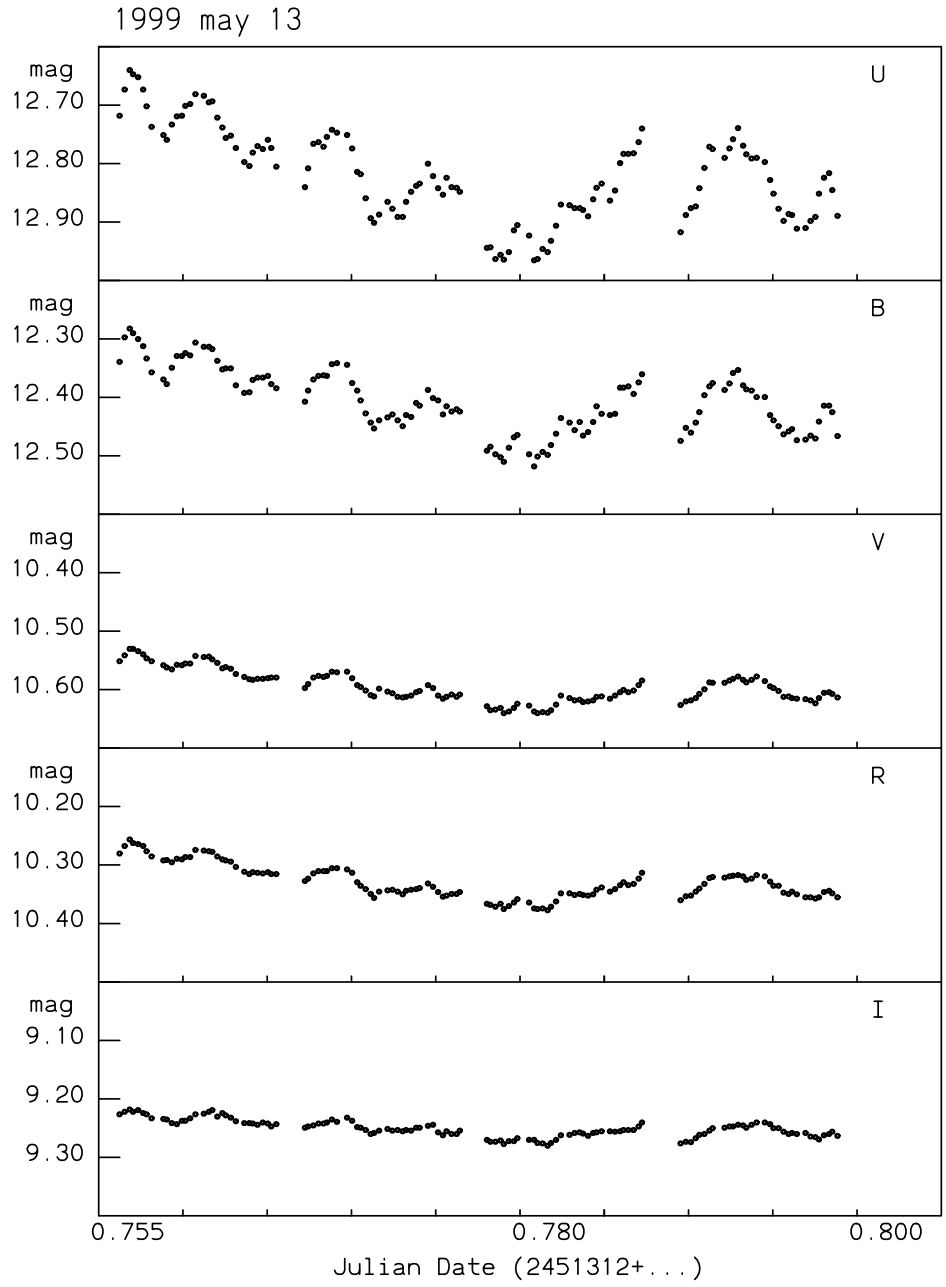

Figure 5: Rapid photometric variations were observed in RS Oph on May 1999. The amplitude of flickering is maximum in the U (ΔU=0.35 mag and ΔB=0.25 mag) and no variations were detected in the VRI bands. This observation was one hour longer and a template star BD-06°4663 was observed before and after RS Oph.

than the red one.

An explanation based on a bipolar gas outflow may be applicable to the presence of these components in the emission lines.
O'Brien et al. (2006) have reported the detection of a spatially resolved structure in RS Oph.
MERLIN radio imaging showed by day 49.4 three components in the direction east-west.
The authors proposed a model that consisted in a bipolar shock-heated shell expanding through the red giant wind with its symmetry axis perpendicular to the plane of the binary orbit.
The low inclination of the orbit supports the possibilty to observe on days 53-55 three emission components in the nebular lines coming from the bright equatorial ring, and two lobes with expanding and receding radial velocities.

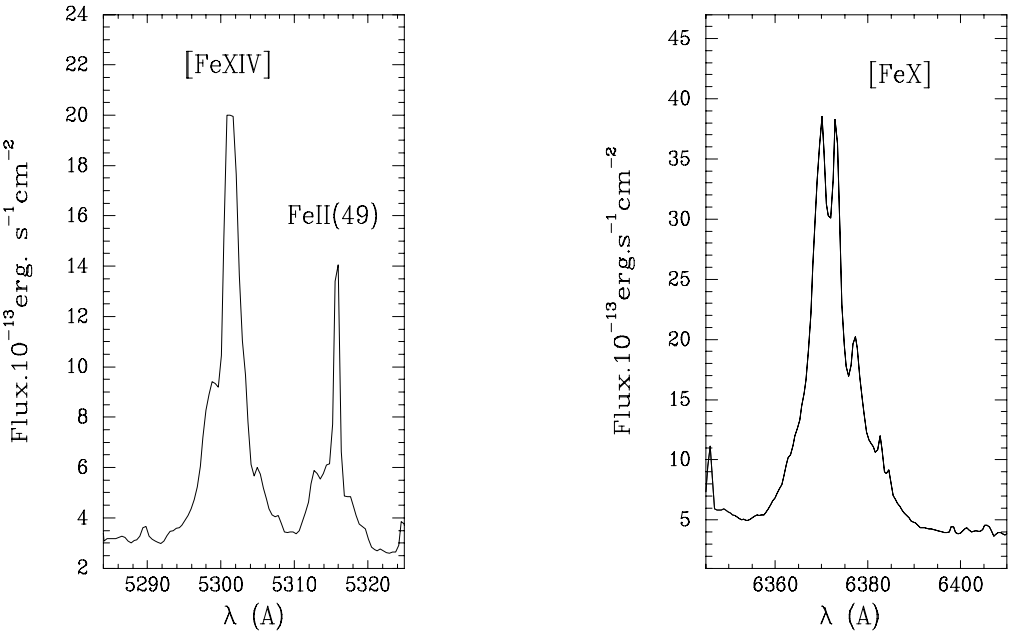

Figure 6: Observed coronal lines on April 2006

5.- RS Oph on October 2006

On October 2006 the RS Oph spectrum is slowly restoring its quiescent characteristics. The intensity of the emission lines decreases, the coronal lines are not observed and the blue and red components of the He I lines have disappeared. Hα presents as incipient the central ab-

sorption which was observed during quiescence (Fig. 3, left panel). A very weak He II λ4686 line is still observed (see Fig. 8) which flux has decreased a factor $\sim$90 respect to that of April. This profile preserves the strong emission component at -46 kms^{-1} and two expanded components at -214 and +192 kms^{-1}, being the red component stronger than the blue one, that is, in opposite sense of that of April.
The cF absorption system is observed again in October 2006.

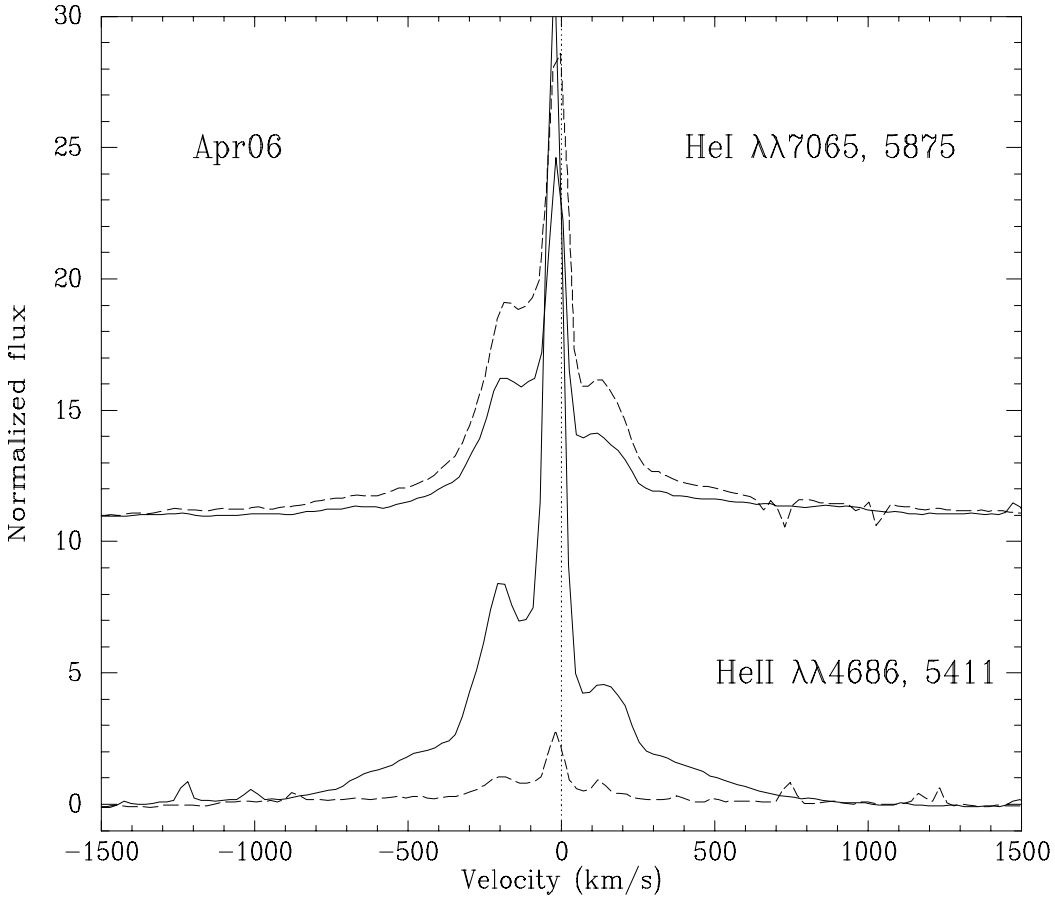

Figure 7: The He I and He II profiles showing a broad pedestal with the strong narrow component at -15 and -23 kms^{-1} respectively. Two separate emission components of higher radial velocity are observed at $\sim$-200 and +150 kms^{-1} being the blue component stronger than the red one.

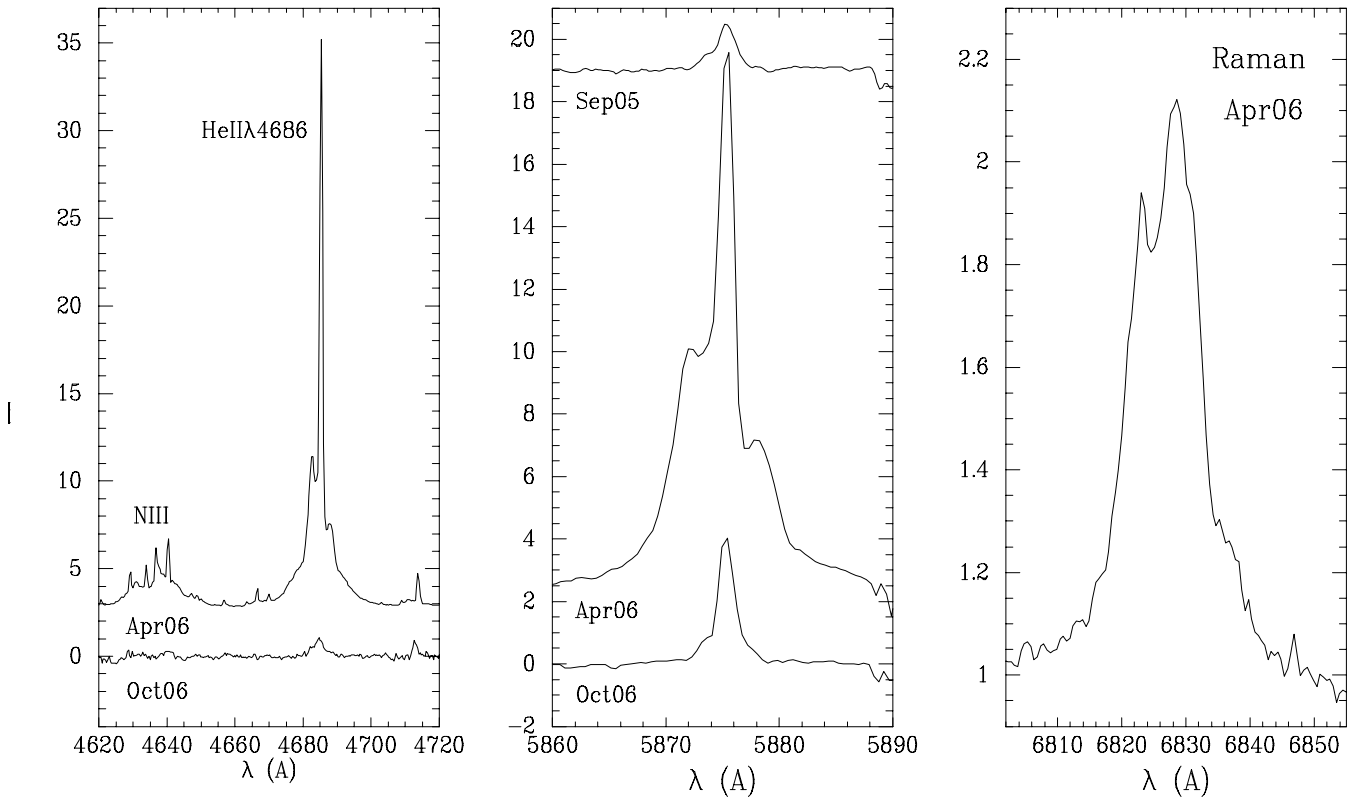

Figure 8: (*left panel*): **N III emission lines are observed on April 2006. The He IIλ4686 is still detected on 2006 October 12.** (*middle panel*): **intensity and profile variations of He Iλ5875 before and after the explosion.** (*right panel*): **the scattering Raman band at 6825 A, which does not appear at all during the quiescent phase, is present as a strong emission profile in April 2006. This feature is not observed in October 2006.**

6.- Conclusions:

- **We have re-determined the spectroscopic orbits based on the radial velocity curves of the M-type absorption lines at wavelengths longer than 6000 Å and of the H I broad emission wings which seem to follow the hot component motion. A period of 453.6 days was determined, very similar to those obtained by F00. We conclude, as DK94 do, that the cF-type absorption lines are not associated with either binary component, and are most likely formed**

in the material streaming towards the hot component. Assuming a massive white dwarf as the hot component of the system ($M_{\rm h} = 1.2 - 1.4 {\rm M}_{\odot}$) the red giant mass results $M_{\rm g} = 0.68 - 0.80 {\rm M}_{\odot}$ and the orbit inclination, $i = 49^{\circ} - 52^{\circ}$.

- **During the quiescent period of our observations the spectra of RS Oph show variability in the fluxes of the emission lines and the continuum. A correlation of the H I and He I emission line fluxes with the monochromatic magnitudes at 4800 Å was obtained, indicating that the hot component activity is responsible of those flux variations. Simultaneous spectroscopic and photometric observations in May 1999 allow us to detect flickering activity in RS Oph, coincident with the relative brightening of the star and the increasing of the emission line fluxes.**
- **We present the characteristics of the spectra around 55 and 240 days following the outburst of February 2006. On April 2006 the most of the emission lines present a broad pedestal with a strong and narrow component at about -20 kms^{-1} and two other extended emission components at -200 and +150 kms^{-1}. These components could be originated in a bipolar gas outflow supporting the model of a bipolar shock-heated shell expanding through the cool component wind and perpendicular to the orbital plane of the binary.**
- **The observations indicate that the cF system was disrupted during the outburst. The cF absorption lines were not observed in our spectra in April 2006 and Zamanov (2006) reported the absence of the flickering in June 2006, then the accretion was not yet resumed immediately after the outburst. Both, the cF system and the flickering (H.**

Worters, poster this meeting) were observed again about 240 days after the outburst which is consistent with the resumption of accretion in RS Oph.

References:

- **Anupama, G.C., Mikołajewska, J. 1999, A&A 344, 177**
- **Brandi, E., Mikołajewska, J., Quiroga, C., Belczyński, K., Ferrer, O.E., García, L.G., Pereira, C.B., 2005, A&A 440, 239**
- **Dobrzycka, D., Kenyon, S., 1994, AJ 108, 2259**
- **Fekel, F., Joyce, R.R., Hinkle, K., 2000, AJ 119, 1375**
- **Mikołajewska, J., Kenyon, S.J., 1992, AJ, 103, 579**
- **O'Brien, T.J., Bode, M.F., Porcas, R.W., Muxlow, T.W.B., Eyres, S.P.S., Beswick, R.J., Garrington, S.T., Davis, R.J., Evans, A. 2006, Nature 442, 279**
- **Quiroga, C., Mikołajewska, J., Brandi, E. et al. 2002, A&A 387, 139**
- **Schneider, D. P., Young, P. 1980, ApJ, 238, 946**
- **Zamanov, R.; Panov, K.; Boer, M.; Coroller, H. Le, 2006, The Astronomer's Telegram 832**

Table 1: Orbital solutions for RS Oph

Component	P [days]	K [kms^{-1}]	γ_0 [kms^{-1}]	e	ω [deg]	$T_\circ^{(1)}$ [JD 24...]	$\Delta\phi^{(2)}$	$a \sin i$ [AU]	$f(M)$ [M$_\odot$]
M-giant									
Our data	452.8±1.5	19.5±0.7	-38.0±0.4	$0^{(3)}$		51055.50		0.81	0.35
Our data	453.2±1.2	20.0±0.7	-38.7±0.4	0.10±0.03	120±16	51205.95		0.83	0.37
DK+F+ours	453.6±0.4	17.5±0.6	-39.5±0.4	$0^{(3)}$		45156.94	0.00	0.73	0.25
DK+F+ours	453.6$^{(3)}$	18.6±0.6	-40.2±0.4	0.14±0.03	135±11	44873.23		0.77	0.29
cF-abs									
Our data$^{(5)}$	453.6$^{(3)}$	8.0±1.2	-32.5±0.9	$0^{(3)}$		50493.51	-0.24	0.33	0.024
	453.6$^{(3)}$	10.2±1.8	-31.8±0.8	0.52±0.14	200±13	50750.54		0.36	0.031
DK+ours	453.6$^{(3)}$	3.2±0.9	-34.7±0.7	$0^{(3)}$		45041.11	-0.26	0.13	0.001
	453.6$^{(3)}$	8.3±2.8	-34.6±0.7	0.82±0.07	344±16	46799.95		0.20	0.005
Emission wings									
Hα wings	456.0±6.1	8.6±1.2	-35.4±0.70	$0^{(3)}$		50376.11			
Hα wings	453.6$^{(3)}$	8.5±1.2	-35.4±0.70	$0^{(3)}$		50385.80	0.53	0.42	0.029
Hα wings$^{(4)}$	453.6$^{(3)}$	10.0±2.3	-36.6±1.5	$0^{(3)}$				0.35	0.047

Combined orbital solutions for RS Oph

Component	P [days]	K [kms^{-1}]	γ_0 [kms^{-1}]	e	ω [deg]	$T_\circ^{(1)}$ [JD24...]	$a \sin i$ [AU]	$M \sin^3$i [M$_\odot$]	q
DK+F+ours	454.1±0.41	17.0±0.6	-38.7±0.4	$0^{(3)}$		45606.67	0.71	0.35	0.59±0.05
Hα wings		10.1±1.2					0.42	0.59	
DK+F+ours	453.6$^{(3)}$	17.1±0.6	-38.7±0.4	$0^{(3)}$		45612.05	0.71	0.35	0.59±0.05
Hα wings		10.1±1.2		$0^{(3)}$			0.42	0.59	
DK+F+ours	453.6$^{(3)}$	17.2±0.7	-38.7±0.4	0.04±0.03	87±44	45722.37	0.72	0.36	0.59±0.05
Hα wings		10.2±1.2					0.42	0.60	
DK+F+ours$^{(4)}$	453.6$^{(3)}$	16.4±1.5	-38.4±0.8	$0^{(3)}$		0.00	0.68	0.35	0.63±0.05
Hα wings$^{(4)}$		10.4±1.8					0.43	0.55	

(1) $T_\circ$ is the time of maximum velocity (circular orbits) or the time of periastron passage (elliptical orbits)

(2) $\Delta\phi$= ($T_\circ$ - $T_\circ g$)/P

(3) assumed

(4) binned data

(5) solutions using only the measurements of the TiII absorption lines.

Table 2: Emission lines of RS Oph on April 2006

Species	λ [Å]	Flux (10^{-12}) ($erg\,s^{-1}\,cm^{-2}$)	RV ($\mathrm{km\,s^{-1}}$) narrow	blue	red	FWZI ($\mathrm{km\,s^{-1}}$)
H I						
Hβ	4861	59.1	-21	-38		2500
Hα	6562	460	-47			3840
P23	8345	0.6	-19			
P22	8359	1.0	-20			
P21	8374	1.0	-23			
P20	8392	1.3	-20			
P19	8413	2.2	-16			
He I						
	4471	2.6	-19	-205	81	1100
	5875	25.4	-14	-194	155	1950
	6678	9.4	-15	-208		740
	7065	28.1	-17	-196	156	1400
He II						
	4686	26.7	-25	-209	164	1680
	5411	3.4	-21	-208	122	1050
Fe II						
M27	4233	1.9	-20	-186		800
M38	4583	1.7	-20	-272:	77w	650
M42	5169	2.3	-20	-121	123w	580
M49	5234	1.4	-22	-124	134	720
M49	5316	2.4	-18	-195	88w	580
M74	6247	0.8	-22	-141	47	514
M73	7711	1.7	-24	-122	181	717
Forbidden lines						
[O I]	6300	0.6	-15	-94	90	350
[N II]	5754	4.6	-42		81	925
[O III]	5007	1.7	-40	-104		320
Coronal lines						
[Fe XIV]	5303	7.0	-52	-220	163w	900
[Fe X]	6375	35.1	-40	-188	166	1500

w: very weak line